Key Points:
- Ocean measurements reveal the impact of solar-derived stored ocean heat on sea ice growth
- Evidence is shown for entrainment of ocean heat in fall/winter by shear and convective mixing
- Release of stored solar heat reduced sea ice thickness at the end of the 2008 growth season by 25%

Correspondence to:
M.-L. Timmermans,
mary-louise.timmermans@yale.edu

The impact of stored solar heat on Arctic sea ice growth

M.-L. Timmermans[1]

[1] Department of Geology and Geophysics, Yale University, New Haven, Connecticut, USA

Abstract High-resolution measurements of ocean temperature and salinity in the Arctic Ocean's Canada Basin reveal the importance of the release of solar-derived stored ocean heat on sea ice growth. Locally absorbed summer solar heat is stored in a near-surface temperature maximum (NSTM) layer underlying the mixed layer. The heat content of the NSTM layer was anomalously large following summer 2007, which saw considerable sea ice losses and intense solar absorption into the exposed surface ocean. Measurements provide evidence for the entrainment of NSTM layer heat in fall/winter 2007–2008 by shear-driven mixing, and convective mixing by the release of dense, salty plumes during sea ice growth. While at least a portion of the NSTM layer was eroded, deeper warm ocean layers remained unaffected. It is shown that the release of solar heat stored following summer 2007 was sufficient to have reduced sea ice thickness at the end of the 2008 growth season by about 25%.

1. Introduction

Enhanced solar heating through open water areas of the upper ocean has played a major role in the extensive losses of Arctic sea ice in recent years, particularly in the Beaufort Sea region [e.g., *Perovich et al.*, 2008; *Comiso et al.*, 2008]. Ice loss is attributed to the ice-albedo feedback mechanism: as ice melts and retreats, heat from the Sun is absorbed into the newly exposed ocean surface, accelerating the rate of melting. While most of the absorbed summer solar heat melts sea ice directly or is lost to the atmosphere, some of the heat is stored in the ocean and released over the course of the following fall and winter [e.g., *Screen and Simmonds*, 2010].

In the summer months when the warmed surface waters melt the sea ice, the melt produces a cold, fresh layer at the surface, giving rise to the formation of an underlying near-surface temperature maximum (NSTM) layer whose heat, derived from the local incoming summer solar radiation, is trapped by stratification and stored [e.g., *McPhee et al.*, 1998; *Perovich et al.*, 2008; *Jackson et al.*, 2010]. Warm water layers deeper than the NSTM layer are another important component of the Arctic Ocean heat budget with implications to sea ice cover. In the Arctic's central Canada Basin; however, the heat in the Pacific and Atlantic water layers is largely insulated from the sea ice cover by the strong halocline stratification [e.g., *Toole et al.*, 2010; *Timmermans et al.*, 2008]. Pacific origin water that is warmed by solar absorption in the Chukchi Sea during the summer (i.e., Pacific Summer Water underlying the NSTM layer, *Coachman and Barnes* [1961]), contains significant heat; however, the temperature of Pacific Summer Water in the central Canada Basin shows no apparent seasonal variability [*Timmermans et al.*, 2014]. On the other hand, the heat content of the NSTM layer, closest to the surface, generally shows a clear seasonal cycle with mixing at the base of the mixed layer in fall as a result of shear or convection, eroding the NSTM layer, and entraining warm water upward [e.g., *Steele et al.*, 2011; *Jackson et al.*, 2012]. *Jackson et al.* [2012], for example, show measurements that indicate brief periods of above-freezing temperatures in the mixed layer (under sea ice) in the fall and winter. They suggest that this is related to entrainment of NSTM layer heat into the mixed layer during anomalously fast sea ice drift events.

Perovich et al. [2008] showed that the solar heat input to the surface ocean was the primary driver of sea ice melt in the Canada Basin region in summer 2007 (the second lowest summer sea ice extent in the satellite record), estimating that the excess solar heat absorption to the surface ocean (as a result of increases in the area fraction of open water) was more than double the amount required to account for the observed 2007 melting of the underside of sea ice. *Perovich et al.* [2008] showed that in some regions of the Beaufort Sea the 2007 total cumulative solar heat input into the ocean was up to 500% more than the average between 1979 and 2005. This raises the important question of whether excess ocean heat was stored in the ocean and the potential consequences of this. Here I examine the impact of the release of stored solar heat on sea
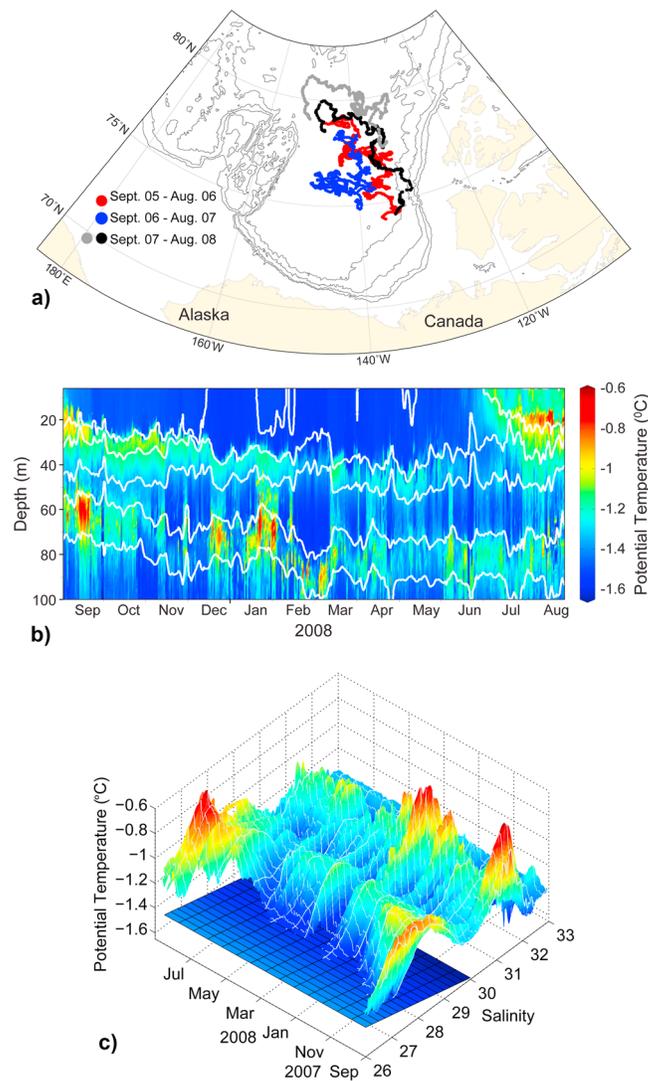
Figure 1. (a) Drift tracks of ITPs that drifted in the Canada Basin (in the region 74°N to 81°N, 130°W to 154°W) between September 2005 and August 2008. In each year, measurements from two ITPs were analyzed (ITP system numbers 1 and 3, 5 and 6, and 8 and 13; see text). (b) Potential temperature-depth time series, where white lines are isohalines (shallowest $S = 28$ in increments of 1), from ITP 8 (grey track in Figure 1a) from September 2007 for a full year. (c) Evolution of $\theta - S$ structure in the upper ocean (measurements shown in Figure 1b), where the gridded plane indicates the freezing temperature plane.

ice growth in the fall and winter in the Canada Basin following the anomalously large solar heat input of summer 2007.

Temperature and salinity measurements from Ice-Tethered Profilers (ITPs) [*Toole et al.*, 2011; *Krishfield et al.*, 2008] operating in the Canada Basin in 2006–2008 are analyzed here (Figure 1a). These data allow for a detailed examination of surface ocean structure under sea ice over a full annual cycle. ITP measurements are described in the next section where a clear delineation is shown between the NSTM layer and the Pacific Summer Water layer that persists throughout the seasonal cycle. In conjunction with ITP measurements, U.S. Army Cold Regions Research and Engineering Laboratory Ice Mass Balance Buoy (IMB) [*Perovich et al.*, 2013] measurements of sea ice bottom melt/growth from the same ice floes are examined in context with solar heat input (section 3). In section 4 the upper ocean signatures of sea ice melt and growth are analyzed to describe mechanisms by which NSTM layer heat content is released. Implications of the release of stored ocean heat are presented in section 5, and results are summarized in section 6.

2. Upper Ocean Temperature and Salinity Measurements

Ocean measurements from beneath the sea ice through the warm layers of the upper ocean are provided by ITPs that operated between September 2005 and August 2008 in the Canada Basin (in a region bounded by 74°N to 81°N and 130°W to 154°W). ITPs are automated profiling systems that are deployed in multiyear ice floes and profile the properties of the underlying ice-covered ocean for periods of up to 3 years [*Krishfield et al.*, 2008; *Toole et al.*, 2011] (http://www.whoi.edu/itp). Temperature, salinity, and pressure sensor accuracies of the final processed measurements (used here) are ±0.001°C, 0.005 and ±1 dbar, respectively. The high resolution of ITP measurements enables a detailed assessment of the upper ocean water mass structure: vertical profile resolution is nominally 25 cm and the ITPs collected between two and four profiles per day (typical ice floe drift speeds are about 10–20 cm/s). The ITP system numbers analyzed here are 1 and 3 (September 2005 to August 2006), 5 and 6 (September 2006 to August 2007), and 8 and 13 (September 2007 to August 2008) (Figure 1a).

The typical upper ocean temperature and salinity structure beneath sea ice in the Beaufort Gyre region over a full annual cycle can be examined from the drift of ITP 8 from August 2007 to August 2008 (Figure 1b). In general, below the base of a ~10 to 30 m deep mixed layer, there is a clear NSTM layer that is both eroded by entrainment and pushed deeper through the fall and winter with seasonal intensification of anticyclonic wind-stress curl and associated Ekman pumping and gyre spin up [*Proshutinsky et al.*, 2009]. Superimposed on this are isopycnal displacements associated with mesoscale eddies and other dynamical processes. This water column heaving can obscure the identification of water mass transformation processes. Isopycnal displacements do not factor, however, when the water column structure is examined in temperature-salinity ($\theta - S$) space (Figure 1c; salinity increases monotonically with depth). In $\theta - S$ space, delineation between the NSTM layer (marked by the shallowest temperature maximum) and underlying Pacific Summer Water layer (the second temperature maximum in depth) becomes clear [see also *Timmermans et al.*, 2014]. There is a general trend of erosion of the NSTM layer, while there is no evidence for erosion of the stratification at the top of the Pacific Summer Water layer, although there is significant spatial variability between profiles. Note also how summer warming drives surface ocean properties off the freezing plane, while in winter, upper ocean layers are shown to remain on the freezing line for a range of salinities.

3. Sea Ice Bottom Melt and Solar Heating

Bottom-melt measurements were provided by IMBs deployed on the same ice floe as ITPs. Each IMB includes acoustic sounders above the ice/snow surface and below the ice bottom to infer sea ice bottom position [*Perovich et al.*, 2013] (http://imb.crrel.usace.army.mil/). I consider bottom-melt measurements from IMBs identified as 2005B and 2007F that were deployed on the same floe as ITPs 3 and 13, respectively. While there was an IMB operating on the same floe as ITP 6 (2006C), the bottom-melt measurements appeared to be anomalous relative to surrounding floes. That is, measurements did not agree with the 2005B and 2007F buoys in the region for overlapping segments of the bottom-melt records, with significantly more melt recorded by 2006C (reported below and in *Perovich et al.* [2008]; *Toole et al.* [2010] employed a 1-D mixed-layer model to show that the 2006C/ITP 6 data in summer 2007 could be interpreted in terms of a closed upper ocean/ice budget). This highlights the strong spatial variability in bottom melt even on regional scales [see *Wettlaufer*, 1991; *Perovich et al.*, 2011b; *Frey et al.*, 2011] but does not affect the conclusions here related to the melt potential of stored ocean heat.

Twice daily downward surface solar radiation data, 2 m air temperature and sea ice concentration data were obtained from the European Centre For Medium-Range Weather Forecasts (ECMWF) ERA-Interim reanalysis product with a resolution of 0.75° [*Dee et al.*, 2011] (this product was also used by *Perovich et al.* [2011a, 2008], and *Zib et al.* [2012] report good comparisons of ERA-Interim reanalyzed surface solar radiation compared with observations in the Arctic) (Figure 2). Areal average values are considered for the region bounded by 74°N to 81°N and 130°W to 154°W. Solar heat input to the ocean F_i is estimated from the surface downward solar irradiance F_s, the albedo of the ocean $\alpha_w \approx 0.07$ [see *Pegau and Paulson*, 2001], and the fractional area of open water A_w as follows

$$F_i = F_s(1 - \alpha_w)A_w. \tag{1}$$

As pointed out by *Perovich et al.* [2008], this estimate is a lower bound as it neglects the effects of sunlight penetration through thin ice. The anomalously large open water area (low sea ice concentration) in this region in summer 2007 resulted in large positive anomalies in solar heat input (Figure 2, middle).
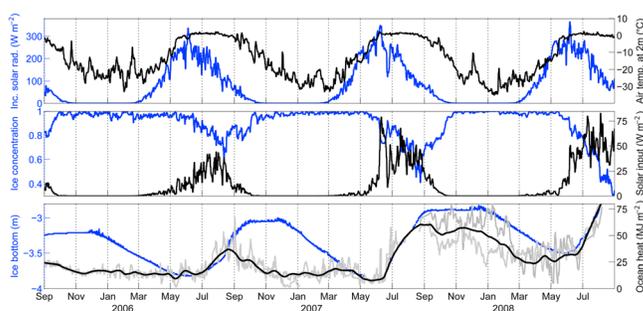
Figure 2. (top) Time series of incident solar radiation (W m^{-2}) and 2 m air temperature (°C) from ERA-40 reanalysis, where values are the areal average in a region bounded by 74°N to 81°N and 130°W to 154°W; (middle) fractional sea ice concentration (averaged over the same area) and solar input to the surface ocean (W m^{-2}, see text for calculation); and (bottom) sea ice bottom position (m) measured by IMBs and ocean heat content (MJ m^{-2}) in the NSTM layer (see text). The grey lines in the bottom panel show ocean heat content for two ITPs in each of the years, and the black line shows the average of these at any given time. Note that most of the bottom melt takes place when the solar warmed water is in contact with sea ice (i.e., before the formation of the summer halocline and underlying NSTM).

The IMBs in the Beaufort Gyre region document periods of sea ice bottom melt between around mid-August and mid-September each year (Figure 2, bottom panel). Over this period bottom-melt rates are about 0.8 cm d^{-1} in the north central Canada Basin [see also *Krishfield et al.*, 2014; *Perovich et al.*, 2008]. This same summer, an IMB deployed around 300 km to the south of these measurements recorded bottom-melt rates up to 11 cm d^{-1} [*Perovich et al.*, 2008], attesting to the large spatial variability in bottom melt in this region. Following the melt period, a relatively stable period of little melt or growth is observed between around mid-September and the end of November. A period of steady sea ice growth takes place between about the end of December and May, with maximum thickness occurring around the end of May each year. Sea ice growth rates in the region are typically around 1/2 cm d^{-1}. Assuming that atmospheric forcing was similar in buoys recording sea ice growth in winters 2005–2006, 2006–2007, and 2007–2008 (Figure 2), the slower growth rate in 2005–2006 compared to 2006–2007 is consistent with the thicker floe in 2005–2006 (latitudinal differences between buoys were less than ∼2°; no snow depth information is available). Further, over the course of winter 2007–2008, the sensor should record more growth (not less) compared to 2006–2007 given that sea ice growth rate is inversely proportional to its thickness. I put forward in section 5 that the anomalously slow ice growth rates in 2007–2008 resulted from the release of stored ocean heat.

4. Ocean Signatures of Sea Ice Melt and Growth

The heat in the NSTM layer can melt or slow the growth of sea ice when it is mixed upward by ice-ocean shear or by convection when sea ice grows. The characteristic temperature-salinity structure corresponding to each of these scenarios will be explored in the following sections.

4.1. Sea Ice Bottom Melt

Shear-driven mixing in the ocean beneath sea ice cover (induced by the relative motion of the ice moving over the surface ocean) can drive entrainment of the NSTM layer at the base of the mixed layer bringing the temperature of the mixed layer (in contact with sea ice) above the freezing point. The warmer water can melt the underside of sea ice or slow its growth depending on concurrent atmospheric forcing. In the case of melt, assuming there is active mixing of the surface ocean layer throughout the melt process (i.e., meltwater does not pool in a boundary layer adjacent to the sea ice), the properties of the product water can be estimated following the seminal results of *Gade* [1979].

When seawater above the freezing temperature (with potential temperature θ_w and S_w, respectively) melts sea ice, the amount by which the water cools and freshens depends upon the latent heat of melting L and the specific heat capacity of water c_w. Considering salt and heat balances, *Moore and Wallace* [1988] (following *Gade* [1979]) derived the following relationship for the salinity S and temperature θ of the product water resulting from melting ice (of salinity S_i)

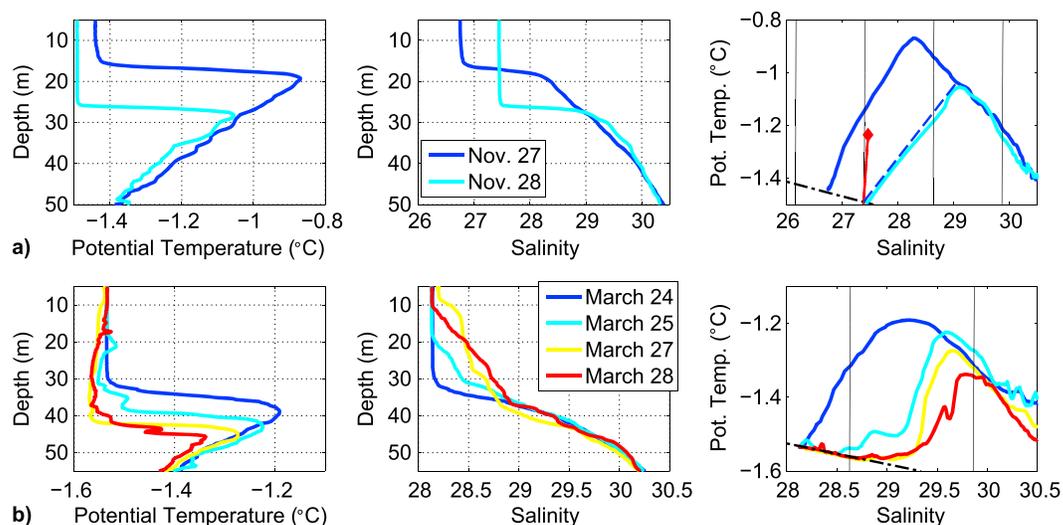$$\frac{\theta - \theta_w}{S - S_w} \approx \frac{L}{c_w}\frac{1}{S_w - S_i}. \tag{2}$$

Figure 3. (left column) Potential temperature (°C) and (middle column) salinity profiles, and (right column) corresponding potential temperature-salinity ($\theta - S$) plots where the solid black lines are contours of potential density relative to the surface, and the dash-dotted line is the freezing line. (a) ITP 13 profiles for the 2007 days shown. The profiles indicate shear-driven mixing and entrainment of a portion of the warm NSTM layer. The red diamond in the right column is the resulting mixed-layer $\theta - S$ derived from homogenizing the initial blue profile to the mixed layer depth of the final cyan profile. The red line is plotted from (2), and its intersection with the freezing line corresponds to the product water of melting sea ice having properties shown by the red diamond. The blue dashed line in the right column is the inferred resulting $\theta - S$ profile. (b) Sequence of profiles from ITP 8 (on the 2008 dates shown) indicating ice growth and the injection of cold, salty plumes into the upper ocean.

Warming of the ice by the underlying water is neglected, and the approximation $(\theta_i c_i / c_w) - \theta_w \ll L/c_w$ has been used where c_i and θ_i are the specific heat and temperature of the ice. Equation (2) is a straight line in $\theta - S$ space where one of the end points is the source temperature and salinity (θ_w and S_w) and the other is the ice salinity S_i and temperature L/c_w. The temperature θ and salinity S of the meltwater mixture lies along this line at the intersection with the freezing line. This formalism was used by *Moore and Wallace* [1988] in considering the thermocline overlying the Atlantic Water layer in the Arctic Ocean. They showed that in this portion of $\theta - S$ space, the slope is consistent with melting by Atlantic Water where it is directly in contact with sea ice (i.e., where it first enters the Arctic Ocean in the Eurasian Basin and surrounding marginal seas). Following *Moore and Wallace* [1988], I take $S_i \approx 7$ (the result is insensitive to the exact value), $\theta_i \approx -1.8°C$, $L = 2.67 \times 10^5 \, J \, kg^{-1}$, and $c_w = 4.05 \times 10^3 \, J \, kg^{-1}°C^{-1}$ to examine water mass transformations in the Beaufort Gyre region associated with shear-driven entrainment of NSTM heat to the underside of sea ice.

Consider the effect of shear-driven mixing, mixed-layer deepening, and entrainment of warm sub-mixed-layer waters of the NSTM layer into the mixed layer. Assume a closed system (i.e., that there is no change to $\theta - S$ other than that produced by melting sea ice), no warming of the ice, and that the conductive heat flux from the atmosphere through the sea ice can be neglected (i.e., all of the heat is used for melting). ITP profiles before and after shear-driven mixing can be analyzed to estimate the presumed melt (Figure 3a). The value of θ_w and S_w may be estimated as the depth average values of the starting profile down to the mixed-layer depth H of the final profile. Assuming all of the entrained heat is used to melt ice yields θ and S of the resulting mixed layer (at the freezing point) from (2). The final profile in $\theta - S$ space can be formed by a line between the final mixed layer properties and the value of $\theta - S$ of the starting profile at the mixed-layer depth of the final profile (Figure 3a). This theoretical profile in $\theta - S$ space predicted by sea ice melt is consistent with the observed profile.

Note that the predicted $\theta - S$ curve would have a steeper slope from the freezing point to the NSTM if it was created by heat removal in the absence of sea ice melt (i.e., sea ice growth is slowed or heat escapes to the atmosphere, and there is only cooling with no change in salinity). The change in this slope with and without melting is within the limitations of what can be measured, particularly given that the system is not closed and there is likely to be some influence of lateral change in mixed-layer freshwater content between successive profiles. Therefore, melt by shear-driven mixing cannot be concluded with certainty solely from

the ITP profiles, although IMB measurements show independent evidence for bottom melt for comparison to melt inferred from temperature-salinity structure.

The amount of bottom melt that results from entrainment of a portion of the NSTM layer can be calculated given the heat content per unit area (relative to the freezing point temperature θ_{fp} corresponding to salinity S_w) in the mixed layer of depth H. If all of the heat is used in ice melt, the resulting ice thickness change is given by

$$\delta h_i = \frac{\rho_w c_w H(\theta_w - \theta_{fp})}{\rho_i L}, \tag{3}$$

where ρ_w and ρ_i are the density of water and ice, respectively. About 6 cm of bottom melt can be inferred from the mixing down of the blue profiles to the cyan profiles in Figure 3a. The IMB on the ice floe with ITP 13 recorded around 4 cm of bottom ablation over the time. Melt inferred from temperature-salinity properties is likely to be larger than measured because there is presumably a nonnegligible conductive flux through the sea ice. Nevertheless, the $\theta - S$ profiles appear to be consistent with shear-driven entrainment and bottom melt.

4.2. Sea Ice Growth

Sea ice growth associated with deepening of the mixed layer will be slowed by the ocean-to-ice heat flux that arises from upward entrainment of the warm NSTM layer. Distinctive winter $\theta - S$ structure of the upper water column provides evidence for sea ice growth and expulsion of brine plumes to the base of the mixed layer and deeper (eroding the NSTM layer) (Figure 3b). The result is a surface layer structure that is entirely at the freezing point and consists of a top homogeneous layer and a lower stratified portion that is saltier and colder. In $\theta - S$ space, the signature of this is a portion of the $\theta - S$ curve lying along the freezing line before peeling off to warmer values (Figures 3b and 1c in winter 2008). In the example shown in Figure 3b, the surface layer in contact with sea ice appears to be isolated from the influence of NSTM layer heat (i.e., its salinity and temperature remain unchanged). The $\theta - S$ structure can be explained as resulting from lateral intrusions associated with nonlocal ice growth. This suggests that the deeper heat must be entrained to the surface at the site of local ice growth, slowing the growth of sea ice there. Whether its influence is local or not, the ice melt equivalent of the entrained heat in this example is about 10 cm. Note that similar $\theta - S$ structures have been attributed to submesoscale eddies [*Timmermans et al.*, 2012], but whether an intrusion or an eddy, the source of the near-surface salty water at freezing point is likely to be sea ice growth.

5. Implications of Stored Ocean Heat

The detailed temperature-salinity structure and the general trends shown in the previous section indicate that heat stored in the NSTM layer is likely to be of consequence to sea ice and illustrate the mechanisms by which it is used up. In this section, I quantify the extent to which the release of stored solar heat melts or inhibits the growth of sea ice over the course of a season. A portion of the cumulative solar heat input to the upper ocean is used to melt sea ice directly, a portion is stored in the ocean, and the remainder is lost to the atmosphere or used to slow the growth of sea ice. The cumulative solar input to the surface ocean (in the region bounded by 74°N to 81°N and 130°W to 154°W) was about 60% more over the 2007 melt season than over the 2006 melt season as a result of the significantly reduced sea ice cover in the region in 2007 (Figure 4). The heat required for the observed bottom melt ($Q = \rho_i \delta h_i L$, from the IMB measurements in Figure 2) was much less than the solar heat absorbed into open water (Figure 4 and see *Perovich et al.* [2008]). In the 2006 melt season, around 20% more heat was absorbed into the upper ocean than used to melt ice, compared to 60% more in the 2007 melt season. These differences are only partly accounted for by additional storage of ocean heat following the 2007 melt season; the majority of excess heat absorbed was likely lost to the atmosphere through open water areas [see, e.g., *Serreze et al.*, 2009].

Ocean heat content (relative to the local freezing temperature) in the NSTM layer is computed by integrating from 10 m depth (for ITP profiles indicating a mixed layer at the freezing temperature deeper than 10 m) to the depth of the temperature minimum at the base of the NSTM layer (Figure 2, bottom). This deep bound ensures the heat content values are not influenced by the heat in the highly spatially and temporally varying Pacific Summer Water below the NSTM layer. While this temperature minimum is subject to a marked deepening over the course of fall and winter associated with the wind-forced dynamics, this does not affect heat content calculations because dynamical deepening is associated with a deepening of the mixed layer (at freezing temperature). Heat content in the NSTM layer was almost twice as large around the end of August 2008 compared to the maximum value the previous August (Figure 2, bottom).
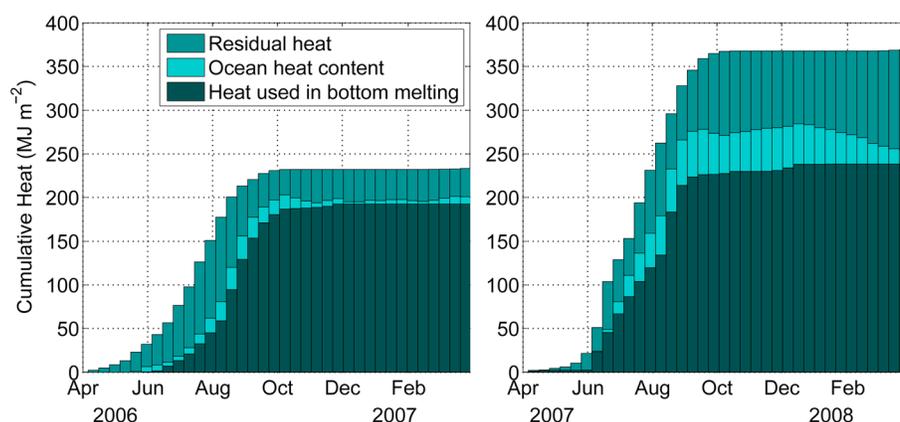
Figure 4. Time series of cumulative heat for (left) 2006–2007 and (right) 2007–2008 for the data shown in Figure 2, where the total height of each bar represents the cumulative solar input to the upper ocean for a bin size of 10 days. The distribution of heat is shown as the sum of heat used to melt ice, the upper ocean heat content (shallower than the warm Pacific layers) in excess of its value at the start of the melt season (computed from the black line in Figure 2, bottom), and the remainder (either heat lost to the atmosphere or heat used to slow the growth of sea ice).

Time series of NSTM layer heat content in excess of the value at the start of the melt season indicate a loss of stored ocean heat from fall 2007 to winter 2008 of around 36 MJ m^{-2} (Figure 4). This heat is equivalent to around 15 cm of ice melt, about one fourth of the total sea ice growth (~60 cm) measured over the 2008 season. By contrast, the ~8 MJ m^{-2} stored ocean heat loss the previous year is equivalent to around 3 cm of ice melt. Coupled with observations that show the release of stored heat (to the surface ocean in contact with sea ice), it is reasonable to conclude that sea ice in May 2008 was a significant fraction thinner than it would have been in the absence of an ocean heat source in winter.

6. Summary

Detailed temperature-salinity structure in the upper ocean reveals anomalously large heat content in the NSTM layer in fall and winter following intensive solar input to the upper ocean during a summer with low sea ice concentration and large areas of open water. This stored heat is mixed upward following the summer season by shear-driven mixing and entrainment or by sea ice growth and rejection of dense, salty plumes. The characteristic $\theta - S$ signatures of these processes have been described. The implication of the release of stored heat is a ~25% reduction in total sea ice thickness (at the end of the 2008 winter growth season). Stored ocean heat likely also impacted winter sea ice growth following the extensive summer melt in the region in 2008 [see, e.g., *Perovich et al.*, 2011b], and this is the subject of a future study. The compound impact of many years of intensive solar absorption and storage is likely to have grave long-term implications to sea ice thickness.

Timing of the solar absorbed heat loss is a key factor in its impact to sea ice. In some recent years, ITP measurements in the Canada Basin have indicated a cooler or absent NSTM layer in fall, likely because it was entirely entrained (by shear-driven mixing) in late summer/early fall. Stored heat has little impact to sea ice if it is released directly to the atmosphere before the onset of the growth season. On the other hand, ocean heat released can delay the onset of freezing. For example, an ocean heat release of 36 MJ m^{-2} could delay freezing by up to a week or so [e.g., *Steele et al.*, 2008].

Anomalously warm Pacific Summer Water layers have also been documented in recent years [*Timmermans et al.*, 2014] — in the absence of an NSTM layer. Future studies are needed to determine whether the stratification at the base of the mixed layer is too strong to allow for shear-driven instability or penetration of plumes below the mixed layer to draw the heat from the Pacific Summer Water layers that have been observed to reside immediately below the mixed layer.

References

Coachman, L., and C. Barnes (1961), The contribution of Bering Sea water to the Arctic Ocean, *Arctic*, *14*, 147–161.
Comiso, J. C., C. L. Parkinson, R. Gersten, and L. Stock (2008), Accelerated decline in the Arctic sea ice cover, *Geophys. Res. Lett.*, *35*, L01703, doi:10.1029/2007GL031972.

Dee, D., et al. (2011), The ERA-Interim reanalysis: Configuration and performance of the data assimilation system, *Q. J. R. Meteorol. Soc.*, *137*(656), 553–597.

Frey, K. E., D. K. Perovich, and B. Light (2011), The spatial distribution of solar radiation under a melting Arctic sea ice cover, *Geophys. Res. Lett.*, *38*, L22501, doi:10.1029/2011GL049421.

Gade, H. G. (1979), Melting of ice in sea water: A primitive model with application to the Antarctic ice shelf and icebergs, *J. Phys. Oceanogr.*, *9*(1), 189–198.

Jackson, J., E. Carmack, F. McLaughlin, S. E. Allen, and R. Ingram (2010), Identification, characterization, and change of the near-surface temperature maximum in the Canada Basin, 1993–2008, *J. Geophys. Res.*, *115*, C05021, doi:10.1029/2009JC005265.

Jackson, J. M., W. J. Williams, and E. C. Carmack (2012), Winter sea-ice melt in the Canada Basin, Arctic Ocean, *Geophys. Res. Lett.*, *39*, L03603, doi:10.1029/2011GL050219.

Krishfield, R., J. Toole, A. Proshutinsky, and M.-L. Timmermans (2008), Automated Ice-Tethered Profilers for seawater observations under pack ice in all seasons, *J. Atmos. Oceanic Technol.*, *25*, 2091–2095.

Krishfield, R. A., A. Proshutinsky, K. Tateyama, W. J. Williams, E. C. Carmack, F. A. McLaughlin, and M.-L. Timmermans (2014), Deterioration of perennial sea ice in the Beaufort Gyre from 2003 to 2012 and its impact on the oceanic freshwater cycle, *J. Geophys. Res. Oceans*, *119*, 1271–1305, doi:10.1002/2013JC008999.

McPhee, M. G., T. P. Stanton, J. H. Morison, and D. G. Martinson (1998), Freshening of the upper ocean in the Arctic: Is perennial sea ice disappearing?, *Geophys. Res. Lett.*, *25*(10), 1729–1732.

Moore, R., and D. Wallace (1988), A relationship between heat transfer to sea ice and temperature-salinity properties of Arctic Ocean waters, *J. Geophys. Res.*, *93*(C1), 565–571.

Pegau, S. W., and C. A. Paulson (2001), The albedo of Arctic leads in summer, *Ann. Glaciol.*, *33*(1), 221–224.

Perovich, D., K. Jones, B. Light, H. Eicken, T. Markus, J. Stroeve, and R. Lindsay (2011a), Solar partitioning in a changing Arctic sea-ice cover, *Ann. Glaciol.*, *52*(57), 192–196.

Perovich, D. K., J. A. Richter-Menge, K. F. Jones, B. Light, B. C. Elder, C. Polashenski, D. Laroche, T. Markus, and R. Lindsay (2011b), Arctic sea-ice melt in 2008 and the role of solar heating, *Ann. Glaciol.*, *52*(57), 355–359.

Perovich, D. K., J. A. Richter-Menge, K. F. Jones, and B. Light (2008), Sunlight, water, and ice: Extreme Arctic sea ice melt during the summer of 2007, *Geophys. Res. Lett.*, *35*, L11501, doi:10.1029/2008GL034007.

Perovich, D. K., J. A. Richter-Menge, B. C. Elder, T. Arbetter, K. Claffey, and C. Polashenski (2013), Observing and understanding climate change: Monitoring the mass balance, motion, and thickness of Arctic sea ice. [Available at http://imb.erdc.dren.mil.]

Proshutinsky, A., R. Krishfield, M.-L. Timmermans, J. Toole, E. Carmack, F. McLaughlin, W. Williams, S. Zimmermann, M. Itoh, and K. Shimada (2009), Beaufort Gyre freshwater reservoir: State and variability from observations, *J. Geophys. Res.*, *114*, C00A10, doi:10.1029/2008JC005104.

Screen, J. A., and I. Simmonds (2010), Increasing fall-winter energy loss from the Arctic Ocean and its role in Arctic temperature amplification, *Geophys. Res. Lett.*, *37*, L16707, doi:10.1029/2010GL044136.

Serreze, M. C., A. Barrett, J. Stroeve, D. Kindig, and M. Holland (2009), The emergence of surface-based Arctic amplification, *The Cryosphere*, *3*(1), 11–19.

Steele, M., W. Ermold, and J. Zhang (2008), Arctic Ocean surface warming trends over the past 100 years, *Geophys. Res. Lett.*, *35*, L02614, doi:10.1029/2007GL031651.

Steele, M., W. Ermold, and J. Zhang (2011), Modeling the formation and fate of the near-surface temperature maximum in the Canadian Basin of the Arctic Ocean, *J. Geophys. Res.*, *116*, C11015, doi:10.1029/2010JC006803.

Timmermans, M.-L., J. Toole, R. Krishfield, and P. Winsor (2008), Ice-Tethered Profiler observations of the double-diffusive staircase in the Canada Basin thermocline, *J. Geophys. Res.*, *113*, C00A02, doi:10.1029/2008JC004829.

Timmermans, M. L., S. Cole, and J. Toole (2012), Horizontal density structure and restratification of the Arctic Ocean surface layer, *J. Phys. Oceanogr.*, *42*(4), 659–668.

Timmermans, M.-L., et al. (2014), Mechanisms of Pacific Summer Water variability in the Arctic's Central Canada Basin, *J. Geophys. Res. Oceans*, *119*, 7523–7548, doi:10.1002/2014JC010273.

Toole, J., M.-L. Timmermans, D. Perovich, R. Krishfield, A. Proshutinsky, and J. Richter-Menge (2010), Influences of the ocean surface mixed layer and thermohaline stratification on Arctic sea ice in the Central Canada Basin, *J. Geophys. Res.*, *115*, C10018, doi:10.1029/2009JC005660.

Toole, J., R. Krishfield, M.-L. Timmermans, and A. Proshutinsky (2011), The ice-tethered profiler: Argo of the Arctic, *Oceanography*, *24*(3), 126–135.

Wettlaufer, J. S. (1991), Heat flux at the ice-ocean interface, *J. Geophys. Res.*, *96*(C4), 7215–7236.

Zib, B., X. Dong, B. Xi, and A. Kennedy (2012), Evaluation and intercomparison of cloud fraction and radiative fluxes in recent reanalyses over the Arctic using BSRN surface observations, *J. Clim.*, *25*(7), 2291–2305.